Master's Thesis

Solvation Structure-Controlled Propylene Carbonate-Based Electrolytes for Lithium Metal Batteries

Daeeun Yu

Department of Energy Engineering

(Battery Science and Technology)

Graduate School of UNIST

2019

Solvation Structure-Controlled Propylene Carbonate-Based Electrolytes for Lithium Metal Batteries

Daeeun Yu

Department of Energy Engineering
(Battery Science and Technology)

Graduate School of UNIST

Solvation Structure-Controlled Propylene Carbonate-Based Electrolytes for Lithium Metal Batteries

A thesis/dissertation
submitted to the Graduate School of UNIST
in partial fulfillment of the
requirements for the degree of
Master of Science

Daeeun Yu

12/06/2018 Month/Day/Year of submission
Approved by

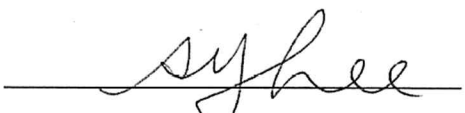

Advisor: Sang-Young Lee

Solvation Structure-Controlled Propylene Carbonate-Based Electrolytes for Lithium Metal Batteries

Daeeun Yu

This certifies that the thesis/dissertation of Daeeun Yu is approved.

12/06/2018 Month/Day/Year of submission

signature

Advisor: Sang-Young Lee

signature

Kyeong-Min Jeong

signature

Nam-Soon Choi

Contents

Abstract

Lithium (Li) metal batteries combined with Ni-rich $LiNi_{0.8}Mn_{0.1}Co_{0.1}O_2$ (NCM811) cathodes have received peculiar attention in respect of their extremely high-energy density. However, since both the Li metal and NCM811 are highly reactive with the electrolytes, unstable Li metal/electrolyte interface and NCM811/electrolyte interface are formed, leading to interfacial side reactions and short cycle life. Furthermore, safety concerns are emerging due to their high risk of explosion.

Here, we designed nonflammable propylene carbonate (PC)-based electrolytes that significantly suppressed the side reactions between the electrodes and electrolytes, *via* manipulating solvation structures of Li ion. At optimal concentration (4 M) of lithium bis(fluorosulfonyl)imide (LiFSI) salt, low amount of free solvent molecules and well-developed ionic association behaviors were shown. Such peculiar solvation structures formed a stable C-N/C-F-rich solid-electrolyte interphase (SEI) layer on the Li metal, which allowed exceptional long-term cycling performance of Li metal along with a high Coulombic efficiency of > 97%. Simultaneously, a stable cathode-electrolyte interphase (CEI) layer was also formed on the NCM811 surface. Driven by the combination of unique passivation layers formed on both electrodes, the Li||NCM811 full cells provide exceptional improvements in electrochemical performance under 3.0 mAh cm^{-2} of high loading cathodes with limited amounts of Li metal, without transition metal (TM) ion dissolutions.

List of figures

Figure 2.8. Nyquist plots of Li||NCM811 full cells. a-b. Nyquist plots of Li||NCM811 full cells in different electrolytes: 1 M LiTFSI-DOL/DME (a) and 4 M LiFSI-PC/FEC (b) at different stages of cycling. The inset is the equivalent circuit.

Figure 2.9. HR-TEM images of the NCM811. a. Pristine NCM811. b-c. The cycled NCM811 (after 100^{th} cycle) in different electrolytes: 1 M LiTFSI-DOL/DME (b) and 4 M LiFSI-PC/FEC (c).

Figure 2.10. Surface analysis performed on cycled NCM811. a-b. XPS spectra of F 1s for CEI layer formed on cycled NCM811 cathodes in 1 M LiTFSI-DOL/DME (a) and 4 M LiFSI-PC/FEC (b). c**.** TOF-SIMS images of $^{7}LiF_2^-$ on cycled NCM811 cathodes in different electrolytes.

Figure 2.11. DSC curves of interfacial exothermic reactions between electrolytes and delithiated NCM811.

Figure 2.12. Comparison of thermal stability of different electrolytes. a. Weight loss of ether-based electrolytes (1 M LiTFSI-DOL/DME and 4 M LiFSI-DME) and 4 M LiFSI-PC/FEC measured by the isothermal TGA at 80 °C for 100 min. b-d. Photographs showing the volatility (top photographs) and inflammability (bottom photographs) of ether-based electrolytes (1 M LiTFSI-DOL/DME (b), 4 M LiFSI-DME (c)) and 4 M LiFSI-PC/FEC (d). The thermal shock test was conducted at 200 °C for 60 min.

List of tables

I. Introduction

1.1. Introduction to lithium ion batteries

A battery is a device that converts the chemical energy into the electrical energy by electrochemical redox reaction. All battery systems contain four main components, an anode, a cathode, a separator and an aqueous/non-aqueous electrolyte. When the battery is connected to an external load, that is, when discharging, the electrons generated by the oxidation reaction of the anode migrate to the cathode *via* the external load and cause a reduction reaction with the cathode materials. At this time, the electric circuit is completed in the electrolyte by the mass transfer of anion and cation in the direction of the anode and the cathode. As the battery is used, the voltage of the battery continues to drop, eventually leading to the failure. At that time, the discarded battery is referred to as a primary battery, and the rechargeable battery is referred to as a secondary battery.

Lithium ion batteries (LIBs) are a type of secondary battery which are attracting much attention as one of the most advanced rechargeable batteries. As their name suggests, LIBs are all about the movement of lithium (Li) ion. Therefore, both anode and cathode allow Li ion to move in and out of their structures with a process called intercalation or de-intercalation, respectively. When discharging, the Li ion move from the anode (usually using graphite (C_6)) to the cathode (usually using lithium transition metal oxide) through the electrolyte. During charge, the conversed reaction occurs (Figure 1.1). The chemical reactions of charge/discharge processes are presented as followed equations.

Graphite (anode) side: $xLi^+ + xe^- + xC_6 \rightleftarrows xLiC_6$ (1)

Lithium cobalt oxide (cathode) side: $LiCoO_2 \rightleftarrows Li_{1-x}CoO_2 + xLi^+ + xe^-$ (2)

Total reaction: $xC_6 + LiCoO_2 \rightleftarrows Li_{1-x}CoO_2 + xLiC$ (3)

(→: Charge reaction, ←: Discharge reaction)

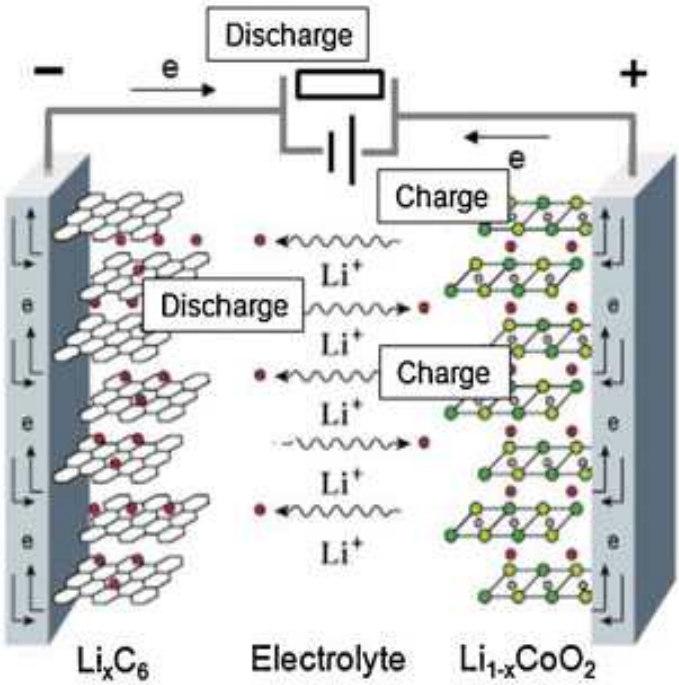

Figure 1.1. A schematic illustration of Li ion batteries consisted of graphite (Li_xC_6) as an anode and lithium cobalt oxide ($Li_{1-x}CoO_2$) as a cathode. Reproduced with permission.[1] Copyright © 2015, Elesvier.

1.2. General requirements of electrolytes for lithium ion batteries

Electrolytes play a role as medium of transport of Li ion between anode and cathode in LIBs. The battery performances, such as the operating voltage and the energy density is theoretically determined by the materials constituting the anode and cathode. However, it is highly important to select the optimum electrolyte because high ion transfer between both electrodes is required to obtain excellent battery performances. Moreover, the electrolytes form a solid-electrolyte interface (SEI) layer at the anode (*i.e.*, graphite and Li-metal) surface during the first Li ion insertion.[2] Once a SEI layer formed, it prevents further side reactions between electrode and the electrolyte, therefore reducing the consumption of electrolyte and irreversible charge loss. Furthermore, the quality of the SEI layer significantly influences rate capability, cycle ability, and safety. That is, it should be again noted that selecting the appropriate electrolyte is essential to improve the battery performances.

The liquid electrolytes in conventional LIBs typically consist of polar organic solvents with dissolved Li salts. Although there are many types of organic solvents and Li salts, the materials that can be used in LIBs are very limited. For liquid electrolytes to be applied to LIBs, the following characteristics are essentially required; (1) The ion conductivity should be high. The higher the ionic conductivity, the better cell performance. Generally, the ionic conductivity required for liquid electrolyte for LIBs is at least 10^{-3} S cm^{-1} at room temperature; (2) It should have a wide electrochemical stability window. The decomposition of electrolyte would not occur within the range of the working potentials of both the anode and cathode. In addition, the electrolyte should be chemically stable not only in the electrodes, but also in other cell components; (3) The available temperature range should be wide; (4) It should be thermally stable. The organic solvents in the electrolyte are generally flammable, and therefore, there is a risk of combustion or explosion when the battery is heated. Accordingly, it is preferable to use the flame retardants or the organic solvents having a high flash point or nonflammable property; (5) It should have low toxicity, because it is possible to be exposed to environment when leakage or disposal.

The characteristics of the electrolytes are determined by the intrinsic properties of the solvents and the Li salts, and can be also significantly influenced by that combination. Table 1.1-1.2 present the physicochemical properties of the solvents and Li salts, respectively.

Table 1.1. Physicochemical properties of representative organic solvents for Li ion batteries.[3]

Solvent	T_m/°C	T_b/°C	η/cP	ε	E_{ox}/V (vs. Li/Li^+)
ethylene carbonate (EC)	39	248	1.86	89.6	6.2
propylene carbonate (PC)	-49.2	241.7	2.53	64.4	6.6
dimethyl carbonate (DMC)	0.5	90	0.59	3.11	6.7
diethyl carbonate (DEC)	-43	126.8	0.75	2.81	6.7
ethyl methyl carbonate (EMC)	-55	108	0.65	2.96	6.7
1,2-dimethoxyethane (DME)	-58	84.7	0.46	7.2	5.1
γ-butyrolactone (GBL)	-42	206	1.75	39.1	8.2
Tetrahydrofuran (THF)	-108.5	65	0.46	7.3	5.2
1,3-dioxolane (DOL)	-95	78	0.58	6.8	5.2
sulfolane (S)	28.9	287.3	9.87	42.5	-
acetonitrile (AN)	-45.7	81.8	0.35	38	-

Table 2.2. Physicochemical properties of representative Li salts for Li ion batteries.[3-5]

Salt	M. Wt/g mol^{-1}	T_m/°C	Al-corrosion	σ/mS cm^{-1} (1.0 M, 25 °C) (in PC)	E_{ox}/V (vs. Li/Li$^+$) (in PC)
$LiPF_6$	151.9	200	N	5.8	6.8
$LiBF_4$	93.9	293	N	3.4	6.6
$LiClO_4$	106.4	236	N	5.6	6.1
$LiAsF_6$	195.9	340	N	5.7	6.8
$Li(CF_3SO_2)_2N$ (LiTFSI)	287.1	228	Y	5.6	6.3
$Li(FSO_2)_2N$ (LiFSI)	187.1	124	Y	5.2	-

II. Solvation Structure-Controlled Propylene Carbonate-Based Electrolytes for Lithium Metal Batteries

2.1. Introduction

The forthcoming electric vehicle era inspires the relentless pursuit of high-energy density batteries (>500 Wh kg^{-1}). Lithium (Li) metal batteries are the promising next-generation energy storage system, because Li metal possess a high specific capacity of 3860 mAh g^{-1} and the lowest potential of -3.04 V (vs. standard hydrogen electrode).[6-7] Li metal coupling with high Ni-content cathode, such as $LiNi_{0.8}Mn_{0.1}Co_{0.1}O_2$ (NCM811), could develop a high-energy density battery that satisfies aforementioned goal.

However, since conventional electrolytes react severely with Li metal and NCM811, unstable and resistive electrode/electrolyte interphase are formed.[2] Unstable Li metal/electrolyte interphase (or solid-electrolyte interphase (SEI)) layer leads to low Coulombic efficiency (CE) and Li dendrite growth.[3, 8-9] Moreover, uncontrolled Li dendrite growth often incurs internal short-circuit during long-term cycling,[10-11] and then battery ignition and explosion may occur due to violently flammable property of the conventional electrolytes.[12] On the NCM811 side, unstable cathode-electrolyte interphase (CEI) layer results in continuous electrolyte decomposition and the transition metal (TM) ion dissolutions. These issues eventually give rise to severe capacity fading.

Various studies have been conducted over the 40 years to address aforementioned issues. The stable passivation layers (*i.e.,* SEI and CEI layer) formed on the electrode surface effectively suppressed further side reactions between electrodes and electrolytes, thereby improving the cycling stability and CE of Li metal batteries. Therefore, many researchers are trying to introduce an electrolyte system that forms a stable passivation layer on the electrode surface. Early investigations of Li metal batteries, the ether-based electrolytes (*e.g.,* 1 M LiTFSI in DOL/DME (1/1 v/v)) was used,[13-17] because the ether solvent exhibit better compatibility with Li metal than carbonate.[18] However, the selection of the cathode is limited, and the risk of battery explosion increases due to their limited oxidation stability (< 4.0 V vs. Li/Li^+) and flammable property of ether solvents.[19-20] Therefore, to commercialize the Li metal batteries, the electrolyte systems having an excellent in oxidative and thermal stability as well as reductive stability are required.

Recently, highly concentrated organic electrolytes are receiving intense attention as a new class of liquid electrolytes because they can achieve striking improvement of both reductive and oxidative stability.[21] In accordance with unique behavior of highly concentrated electrolytes, C. Wang et al. simultaneously stabilized both Li metal and NCM622 with highly concentrated EC/DEC-based electrolyte by forming a fluorinated passivation layer on both electrodes surface.[22] Also, W. Xu et al. effectively overcame the oxidative stability limit of ether solvents by using dual-salt and increasing

electrolyte concentration.[23] This electrolyte system could sacrificially passivate NCM111 and thus mitigated the oxidation of electrolytes. Furthermore, since it formed a stable SEI layer on the Li metal for efficient Li metal cycling, they achieved excellent cyclability of Li||NCM111. Even if Li metal batteries could be realized using these electrolyte systems, it is still difficult to be commercialized due to their limited thermal stability. In addition, they are only applied to cathode with low Ni content (< 80%), which is insufficient to fulfil the high-energy density batteries.

Although various studies have been conducted to achieve Li metal batteries as described above, previous papers use very thick Li metal (> 50 μm) and cathodes with low-loading level (< 2.0 mAh cm^{-2}).[22-27] Since the cycle life of Li metal batteries depends on the degree of capacity utilization of Li metal,[28] the use of thick Li metal and cathodes with low-loading level, as in the previous papers, has no meaningful cycle life. So far, as the improvement in cycle performance of Li metal batteries was more important, the degree of capacity utilization has been overlooked. Recently, C. Wang et al., Li||NCM811 full cells using limited amounts of Li-metal was achieved.[29] However, the loading of the cathodes is only 2 mAh cm^{-2}, which is inadequate for practical applications. Consequently, to realize the realistic high-energy density Li-metal batteries, it is necessary to use limited amounts of Li metal and cathodes with high-loading level (≥ 3.0 mAh cm^{-2}).

Here, we report a highly efficient approach to achieve the high-energy density and high-safe Li metal batteries *via* controlling solvation structures of Li ion with a suitable salt/solvent combination. We use propylene carbonate (PC) as a solvent, which has excellent thermal and oxidative stability,[3] and lithium bis(fluorosulfonyl)imide (LiFSI) salt, which is well known to form a stable SEI layer on the surface of the Li metal. To further improving the stability of the SEI layer, we also added 7% (by volume) of fluoroethylene carbonate (FEC), which can be polymerized on the Li metal surface and sturdily bound the inorganic compounds of SEI layer.[30] This nonflammable electrolyte system formed a stable C-N/C-F-rich SEI layer on the surface of Li metal, when the concentration of LiFSI is 4 M. The C-N/C-F-rich SEI layer allows exceptional long-term cycling stability of Li||Li symmetric cell over 2,500 h, along with limited polarization increase. Also, a stable CEI layer was formed on the NCM811 surface, which successfully suppressed oxidative decomposition of electrolytes and TM ion dissolutions. The combination of unique stabilization on both Li metal and NCM811 enabled the outstanding cycling stability of Li||NCM811 full cells (86% retention at the 100th cycle), when the thin Li metal (20 μm) and NCM811 with high-loading level (3.0 mAh cm^{-2}) were used (73% of capacity utilization of Li metal).

2.2. Experimental

2.2.1. Materials

Li foils with a thickness of 200 μm were purchased from Honjo Chemical Co. Li foil of 20 μm thickness and NCM811 ($LiNi_{0.8}Mn_{0.1}Co_{0.1}O_2$) active materials were kindly provided from LG Chemical Co. The laminate of NCM811 electrode (~13.8 mg cm^{-2}) was fabricated by casting NMP-based slurry mixture containing 90 wt% of NCM811 active material, 5 wt% of super P (conductive material) and 5 wt% of polyvinylidene fluoride (PVdF) binder on an aluminum current collector. After drying at 120 ºC, the electrodes were laminated by roll pressing machine. Propylene carbonate (PC), fluoroethylene carbonate (FEC), and 1,3-dioxolane (DOL) were bought from Sigma-Aldrich and 1,2-dimethoxyethane (DME) was purchased from TCI Co. Lithium bis(fluorosulfonyl)imide (LiFSI) salts were obtained from LG Chemical Co. and Lithium bis(trifluoromethanesulfonyl)imide (LiTFSI) salts were bought from Enchem Co. The salts dried under 120 ºC and vacuum conditions before use. To make electrolytes, PC and FEC were mixed by 93/7 volume ratio, and then calculated amounts of LiFSI salts were fully dissolved into the PC/FEC solvent mixture. In the same way, DOL and DME were mixed first (1/1 v/v) and then calculated amounts of LiTFSI salts were added accordingly. These chemicals were kept and handled in an Ar-filled glovebox.

2.2.2. Electrochemical measurements

All of charge/discharge performances were measured using 2032-type coin cell with cycle testers (PNE Solution) at room temperature. Due to the corrosion of stainless steel in LiFSI-PC/FEC, Al-clad cases obtained from LG Chemical Co. were used. Li||Li symmetric cells were constructed using the Li metal foil of 20 μm thickness, the prepared electrolyte (100 μl in each cell), and two pieces of polyethylene (PE) separator (Celgard 3501). The long-term cycle life test of Li||Li symmetric cells was conducted at a current density of 0.2 mA cm^{-2} with an areal capacity of 0.5 mAh cm^{-2}. The EIS of Li||Li symmetric cells was examined using a potentiostat (VSP classic, Bio-Logic), where the frequency range is 10^{-2} to 10^{6} Hz at an amplitude of 10 mV. For the Li||NCM811 full cells with "1.4×excess" Li-metal, the Li-metal was pre-deposited on the Cu current collector. To remove possible oxidation layer, the Cu was pre-cycled for 5 cycles before deposition. The volume of the electrolyte in the Li||NCM811 full cells was 100 μl and one piece of PE separator was used. The Li||NCM811 full cells were tested between 3.0 and 4.2 V. The EIS of Li||NCM811 full cells was examined where the frequency range is 10^{-3} to 10^{6} Hz at an amplitude of 10 mV. A three-electrode cell was used to examine the oxidation stability window for the different electrolytes at a scanning rate of 0.1 mV s^{-2}. Platinum (Pt) rod was used as a working electrode, Pt coil was used as a counter electrode, and Li metal was used as a reference electrode.

2.2.3. Characterizations

To investigate the solvation structures of Li ion in the electrolytes, Raman spectra (alpha300S, WITec) were recorded by using a laser to excite at 532 nm. The electrolytes were put into two glass plates and tightly sealed in an Ar-filled glove box to prevent any contamination from the air. XPS (K-alpha, ThermoFisher) was conducted on the cycled Li metal and NCM811 with monochromatized Al Kα radiation. The sp^2 C peak (284.5 eV) was used as the reference peak to calibrate other values. SEM (S-4800, Hitachi) measurements were performed on cycled Li metal after 20^{th} depositions with an electron accelerating voltage of 10 kV. Before the characterizations, the Li metal was rinsed by dimethyl carbonate (DMC) and dried. HR-TEM (JEM-2100F, JEOL) analysis were conducted on NCM811 particles after 100^{th} cycles. TOF-SIMS (TOF-SIMS 5, ION TOF) was performed to analyze the TM ion dissolutions on the NCM811 surface after cycling test with Bi_3^{2+} gun at 50 keV. TGA (Q500, TA) with isothermal mode at 80 ºC for 100 min was used to estimate the weight loss of the electrolytes as a function of time. The interfacial exothermic reaction between the electrolytes and delithiated NCM811 was inspected by DSC measurements (Q200, TA). The samples transferred to high-pressure pan and heated at a scanning rate of 5 °C min^{-1}.

2.3. Results and discussion

2.3.1. SEI layer evolution and lithium metal protection effect

The solvation behavior and ionic association of the LiFSI-PC/FEC (93/7 v/v) depending on LiFSI concentrations were elucidated by conducting Raman analysis (Figure 2.1a). The Raman spectra shows a symmetric ring deformation vibration band at 712 cm^{-1}, which is deriving from free PC molecules. When the PC molecules participate in the solvation structure of Li ion, this band shifts up to 722 cm^{-1} as shown in Figure 2.1a.[31] As expected, increasing the LiFSI concentration, the fraction of PC molecules coordinated with Li ion increase. Furthermore, the Li^{+}-FSI^{-} association simultaneously intensified with a lack of PC molecules to retain a stable fourfold coordination.[32] Therefore, with increasing LiFSI concentration, the free FSI^{-} anions decrease and disappear to form contact ion pairs (CIPs, FSI^{-} coordinating to one Li ion), aggregate clusters-I (AGGs-I, FSI^{-} coordinating to two Li ion), and aggregate cluster-II (AGGs-II, FSI^{-} coordinating to three Li ion).[33-34] This is evidenced from a remarkable upshift of the FSI^{-} band from 720 cm^{-1} to 732, 746, and 769 cm^{-1}. Accordingly, there is a striking difference in the solvation structure between 1, 4 and 5 M concentrations; the majority of PC molecules exist in a free state at 1 M, whereas at 4 and 5 M, all of the PC molecules coordinate to Li ion and there are no free PC molecules. Moreover, almost FSI^{-} anions properly coexist as CIPs and AGGs-I state at 4 M. However, AGGs-I and AGGs-II state, which form macromolecules in electrolytes,[35] are dominant at the 5 M. The modified SEI layer-forming ability of electrolytes can be provided by these peculiar structural features.[36-38]

X-ray photoelectron spectroscopy (XPS) analysis unveiled the components of the SEI layer formed on the surface of Li metal cycled in different concentrations (Figure 2.1b-c). The differences in the C 1s and F 1s spectra between the three Li metal that were cycled in 1, 4, and 5 M LiFSI-PC/FEC are pronounced. The SEI layer formed at the 1 M was enriched with common carbonaceous species (sp^2 C (284.5 eV), C-O (286.0 eV), O-C=O (288.1 eV), and CO_3^{2-} (289.0 eV)). These species could have originated from decomposition products of PC molecules.[39] Although LiF, which derived from LiFSI and FEC, was contained, organic components existed dominantly. Since the SEI layer enriched with organic components is porous, electrolytes can be diffused through their pores and be reduced continuously.[40] On the other hand, two peculiar peaks (287.2 eV and 291.0 eV) assigned to C-N and C-F species were observed at 4 M, whereas the amount of carbonaceous components is relatively small. This is because reductive reactions of PC molecules on the Li metal could be mitigated, due to the absence of free PC molecules. Also, another possibility is that C_3H_6, may react with $N(SO_2F_2)$, which are decomposition products of the PC and LiFSI respectively, to form polymeric C-N and C-F components. Moreover, inorganic components, such as $LiSO_2F$ and LiF, is properly exist in the SEI layer. Since they can form relatively dense SEI layer, they are well known that the key components of an effective passivation layer to protect Li metal.[40] Therefore, we can tentatively conclude that the SEI layer was

formed, which inorganic components are densely packed on the Li metal surface and the polymeric C-N and C-F components are bound the inorganic components well. Interestingly, at the 5 M, similar behavior to 1 M appeared. Although there are no free PC molecules at the 5 M, a SEI layer enriched with the common carbonaceous species was formed. As mentioned above, the SEI layer is expected to have low Li metal protection effect as it cannot effectively prevent side reactions between Li metal and electrolytes. This unusual behavior seems to be related to the solvation behavior of Li ion, which requires further study. To gain insight into the Li metal protection effect of these SEI layers, electrochemical properties will be in-depth investigated in the next part.

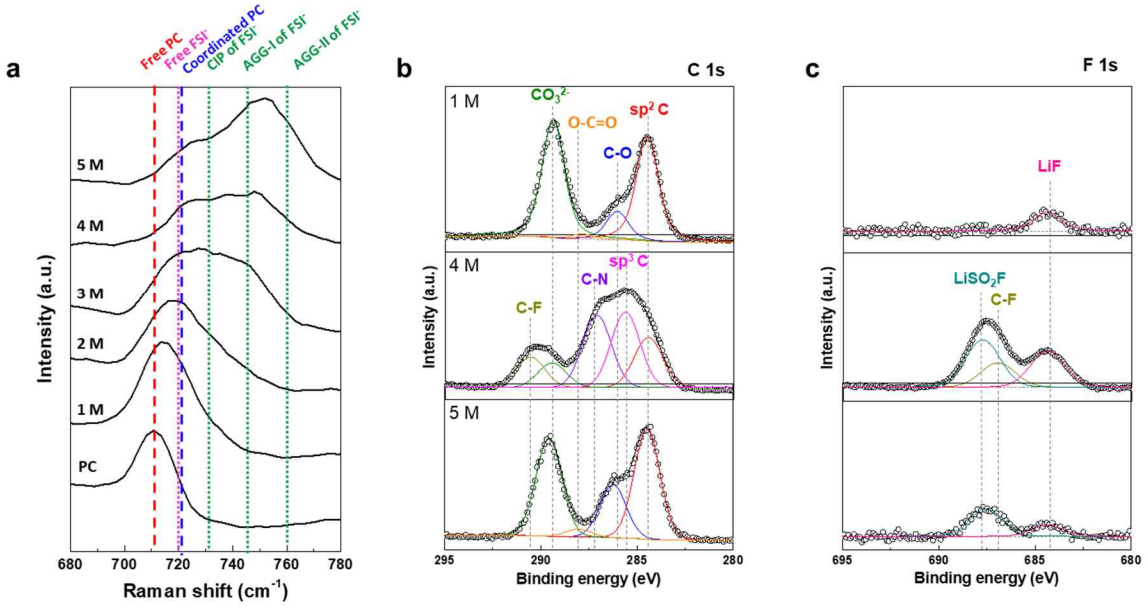

Figure 2.1. The effect of LiFSI concentration on solvation structures and SEI layer components. a. Raman spectra of LiFSI-PC/FEC electrolyte with different concentrations in the region 680 and 780 cm^{-1}. b-c. XPS spectra of C 1s (b) and F 1s (c) for SEI layer formed on the Li metal cycled in 1 M, 4 M, and 5 M LiFSI-PC/FEC.

We assembled Li||Li symmetric cells to further confirm the Li metal protection effect of SEI layers formed differently depending on the LiFSI concentrations. First, we conducted galvanostatic cycling test to elucidate how effectively the SEI layers prevent the reductive side reactions of electrolytes during long-term cycling (Figure 2.2a). The Li||Li cell with 1 M LiFSI-PC/FEC exhibits fast increasing the overpotential and then failed after ~130 h. Although relatively stable cycling behavior was achieved at the 5 M, the overpotential continuously increased and failed after ~1800 h. This is because the organic component-dominant SEI layer could not insulate contact between the Li metal and electrolytes, and finally electrolyte depletion occurred due to the continuous consumption of the electrolytes.[41] In contrast, at the same current density, the Li||Li cell at the 4 M was achieved the exceptional long-term cycling stability over 2,500 h, along with limited overpotential increase. This result suggests that the C-N/C-F-rich SEI layer could effectively prevent the attack by the electrolytes.

To gain basic insight into the SEI layers, we next performed electrochemical impedance spectroscopy (EIS) measurements on the Li||Li cells (Figure 2.2b). The evolution of the EIS upon an open-circuit rest provides robust evidence of ionic conductivity and resistance of the SEI layer.[42] In the equivalent circuit (Figure 2.2c), R_s, R_{int} and R_{ct} are attributed to the electrolyte resistance, SEI layer resistance and charge transference resistance, respectively. Within a 30 min rest, the Li||Li cell at the 4 M showed extremely low R_{int} (16.2 Ω) and R_{ct} (10.5 Ω), while very high R_{int} and R_{ct} was exhibited at the 1 and 5 M. All the values of resistance are listed in Table 2.1. The very minor R_{int} and R_{ct} at the 4 M supports the C-N/C-F-rich SEI layer has the ability to enhance Li ion migration near the Li metal/electrolyte interface and enables stable operation of the Li||Li cells observed experimentally. In contrast, the SEI layers formed at 1 and 5 M has high resistance to the migration of Li ion, leading to uneven Li ion deposition behavior.

Scanning electron microscopy (SEM) images in Figure 2.3 compared the Li metal surfaces after being cycled in different electrolytes. Significant amount of needle-like dendrites as well as dead Li formed on the surface of the Li metal anode during cycling at the 1 M (Figure 2.3a). This morphology increases the specific surface area of the Li metal, accelerating the side reactions between the Li metal and the electrolytes.[43] This results in poor cycling stability as shown in the galvanostatic cycling result (Figure 2.2a). In addition, at 5 M, fractal dendrites, which exacerbate the risk of battery short-circuit,[44] were grown on a roundly deposited surface (Figure 2.3c). However, the Li metal surface cycled in 4 M LiFSI-PC/FEC displayed an uniform and dense structure with a round shaped deposition morphology (Figure 2.3b). Such morphology of Li metal could significantly relieve safety concern and minimized side reactions of electrolytes.[22]

Benefiting from the C-N/C-F-rich SEI layer, the 4 M LiFSI-PC/FEC also considerably improved the Coulombic efficiency (CE) of Li stripping/plating. At current density of 0.2 mA cm^{-2}, the CE at 4 M increases to > 97% within 50 cycles and remains over 100 cycles (Figure 2.4). In contrast,

the CE at 1 M showed very unstable behavior and dropped to 10% after 40 cycles. Although comparative high CE of ~ 95% was attained at 5 M for the initial cycles, it continuously decreased and reached 88%. From the above mentioned electrochemical performances demonstrated that the C-N/C-F-rich SEI layer formed at 4 M LiFSI-PC/FEC has excellent Li metal protection effect.

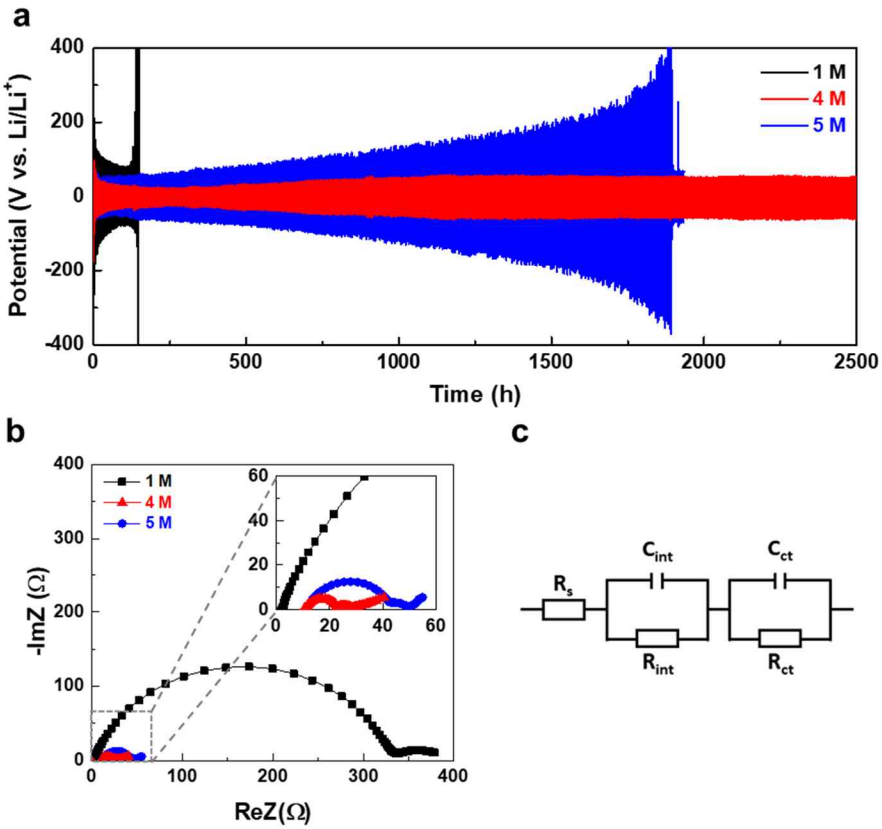

Figure 2.2. Electrochemical behavior of Li||Li symmetric cells in different electrolytes. a. Long-term cycling of Li||Li symmetric cells with 1 M, 4 M, and 5 M LiFSI-PC/FEC at current density of 0.2 mA cm^{-2} with an areal capacity of 0.5 mAh cm^{-2}. b. Nyquist plots of Li||Li symmetric cells with different salt concentrations (1 M, 4 M, and 5 M) at open circuit. c. Corresponding equivalent circuit used to fit the Nyquist plot.

Table 2.3. Resistance values obtained from Nyquist plots of Li||Li symmetric cells in Figure 2.2b.

	R_s (Ω)	R_{int} (Ω)	R_{ct} (Ω)
1 M LiFSI-PC/FEC (93/7 v/v)	2.1	333.5	42.6
4 M LiFSI-PC/FEC (93/7 v/v)	10.4	16.2	10.5
5 M LiFSI-PC/FEC (93/7 v/v)	11.8	31.3	7.2

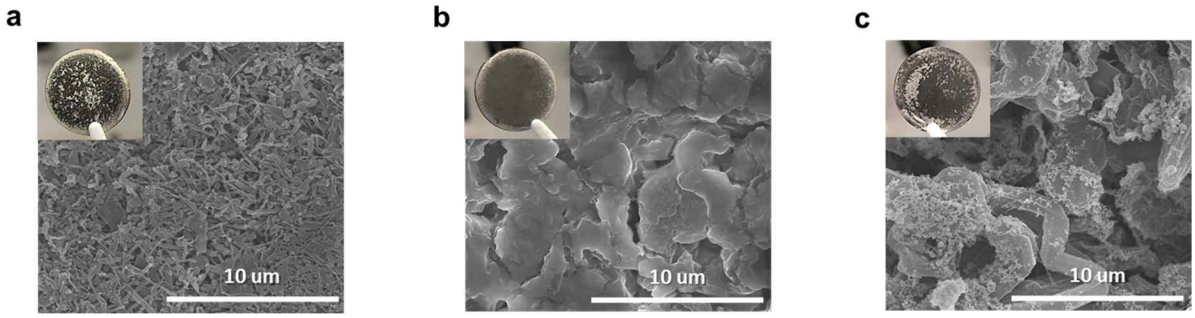

Figure 2.3. Morphology of cycled Li metal. a-c. SEM and optical images (insets) of Li metal cycled in 1 M (a), 4 M (b), and 5 M (c) LiFSI-PC/FEC.

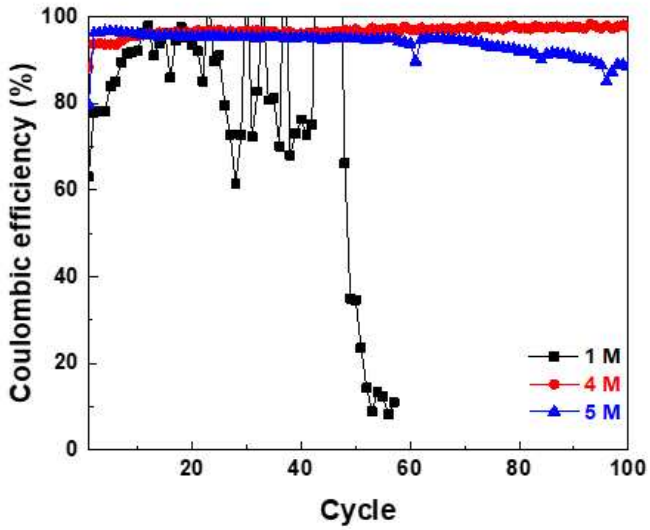

Figure 2.4. Coulombic efficiency of Li plating/stripping in different electrolytes. Coulombic efficiency of Li plating/stripping at current density of 0.2 mA cm^{-2} with areal capacity of 0.5 mAh cm^{-2} in 1 M, 4 M, and 5 M LiFSI-PC/FEC.

2.3.2. The electrochemical performance of Li||NCM811 full cell

Linear sweep voltammetry (LSV) was performed using a three-electrode cell with platinum (Pt) rod as a working electrode to evaluate the oxidation stability of various electrolytes (Figure 2.5). Ether-based electrolytes which well known that relatively stable to Li metal, showed a narrow oxidation stability window, as evidenced by a rapid increase in current above 3.8 V. The feature of easy oxidation renders the ether-based electrolytes cannot be utilized in the higher voltage systems (> 4 V),[19,29] while it has a stable Li plating/stripping behavior. Although 1 M LiFSI-PC/FEC displayed more stable behavior against oxidation compared to 1 M LiTFSI-DOL/DME, a high anodic current was still observed above 4.5 V. In contrast, even at 5.5 V, low anodic current was observed for 4 M LiFSI-PC/FEC. The significant improvement of the oxidation stability can be attributed to two reasons. First, there are no free PC molecules oxidized near 4.5 V at the 4 M. Second, the PC molecules coordinated with Li ion may have a lower tendency to be oxidized due to the donation of the lone pair on oxygen atoms. In summary, the 4 M LiFSI-PC/FEC showed salient stability towards not only the Li metal but also high-voltage cathodes.

Accordingly, we constructed Li metal full cells using NCM811 with 4 M LiFSI-PC/FEC to achieve high-energy density batteries. Although various studies have been conducted to demonstrate Li metal batteries, previous papers use very thick Li metal (> 50 um) (Table 2.2). Li metal batteries using thick Li metal show very low energy density (Wh kg^{-1}). In addition, since the cycle life of the Li metal batteries depends on the degree of capacity utilization of Li metal, the use of thick Li metal as in the previous papers enables to achieve untruth excellent long-term cyclability (Figure 2.6). Even if a couple of papers use a thin Li metal, the loading of the cathodes is low (< 2.0 mAh cm^{-2}). This is insufficient for practical applications. As a result, thin Li metal (< 20 um) and cathodes with high loading level (≥ 3.0 mAh cm^{-2}) should be used to achieve the realistic high-energy density Li metal batteries. Therefore, we used a thin Li metal of 20 μm and NCM811 of 3.0 mAh cm^{-2}.

The electrochemical performances of the Li||NCM811 full cells with different electrolytes cycled between 3.0 and 4.2 V at 0.3 mA cm^{-2} are shown in Figure 2.7. All of the cells exhibited nearly the same initial discharge capacity (185 mAh g^{-1}). However, the Li||NCM811 cell using the 1 M LiTFSI-DOL/DME exhibited fast capacity fading after 10^{th} cycles. In addition, they showed gradual voltage polarization increases (Figure 2.7b). This can be ascribed to increasing cell resistance owing to oxidative decomposition of electrolyte. In contrast, the Li||NCM811 cell with the 4 M LiFSI-PC/FEC displayed stable cycling with < 86% capacity retention after 100 cycles, along with average Coulombic efficiency close to 99.5% (Figure 2.7c). More importantly, it displayed very limited increase of polarization, with very stable charge/discharge voltage profile (Figure 2.7c). The voltage polarization increase mechanism was investigated by EIS (Figure 2.8). Both R_{int} and R_{ct} values of Li||NCM811 cell using 1 M LiTFSI-DOL/DME are very large in 5^{th} cycle. And these values largely increased within

10 cycles (Figure 2.8a), indicating that consumption of electrolyte occurred continuously at NCM811 and the resistive and thick CEI layer was formed. On the other hand, Li||NCM811 cell using 4 M LiFSI-PC/FEC showed relatively low R_{int} and R_{ct} values in 5th cycle. Also, both values decreased within 100 cycles (Figure 2.8b), which signified that more ionically conductive and stable CEI layer was formed.[28]

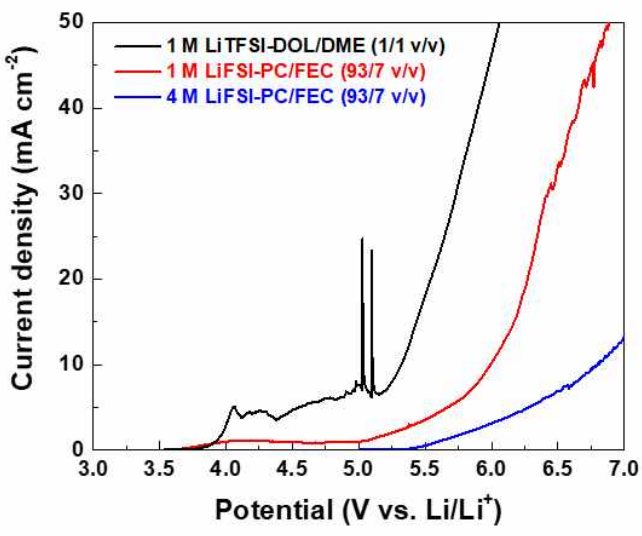

Figure 2.5. Oxidation stability of different electrolytes. Oxidation stability of different electrolytes as evaluated on platinum (Pt) electrode at a scanning rate of 0.1 mV s^{-1}.

Table 2.4. Summary of representative papers about electrolyte design for Li metal batteries.

Cell configuration	Electrolyte	Thickness of Li-metal (μm)	Cathode loading level (mAh cm^{-2})	N/P ratio	Energy density (Wh kg^{-1})	Ref.
Li‖NCM622	1 M $LiPF_6$ in FEC/DMC	50	3.3	3.1	-	45
Li‖NCM424	0.6 M LiTFSI + 0.4 M LiBOB in EC/EMC + 0.05 M $LiPF_6$	120	1.75	14.1	-	25
Li‖LNMO	7 M LiFSI in FEC	2.55 mAh cm^{-2}	1.83	1.4	583	46
Li‖NCM622	10 M LiFSI in EC/DMC	-	2.5	-	-	22
Li‖NCM76	0.6 M LiTFSI + 0.4 M LiBOB in EC/EMC + 0.05 M $LiPF_6$	450	0.8	115.9	-	26
Li‖NCM622	1.2 M LiFSI-TEP/BTFE	450	1.6	58.0	-	27
Li‖NCM111	2 M LiTFSI + 2 M LiDFOB-DME	250	1.7	30.3	-	23
Li‖NCM811	1 M $LiPF_6$ in FEC/FEMC/HFE	2 mAh cm^{-2}	2	1	680	29

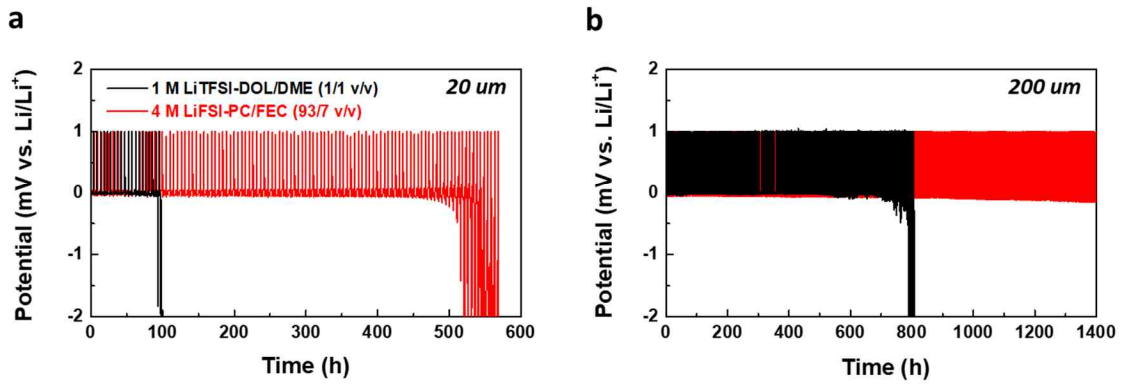

Figure 2.6. Cycle life of Li||Cu cells for different thickness of Li metal. a-b. Li metal plating/stripping profiles on a Cu working electrode cycled in different electrolytes: 1 M LiTFSI-DOL/DME and 4 M LiFSI-PC/FEC with 20 μm of Li metal (a) and 200 μm of Li metal (b).

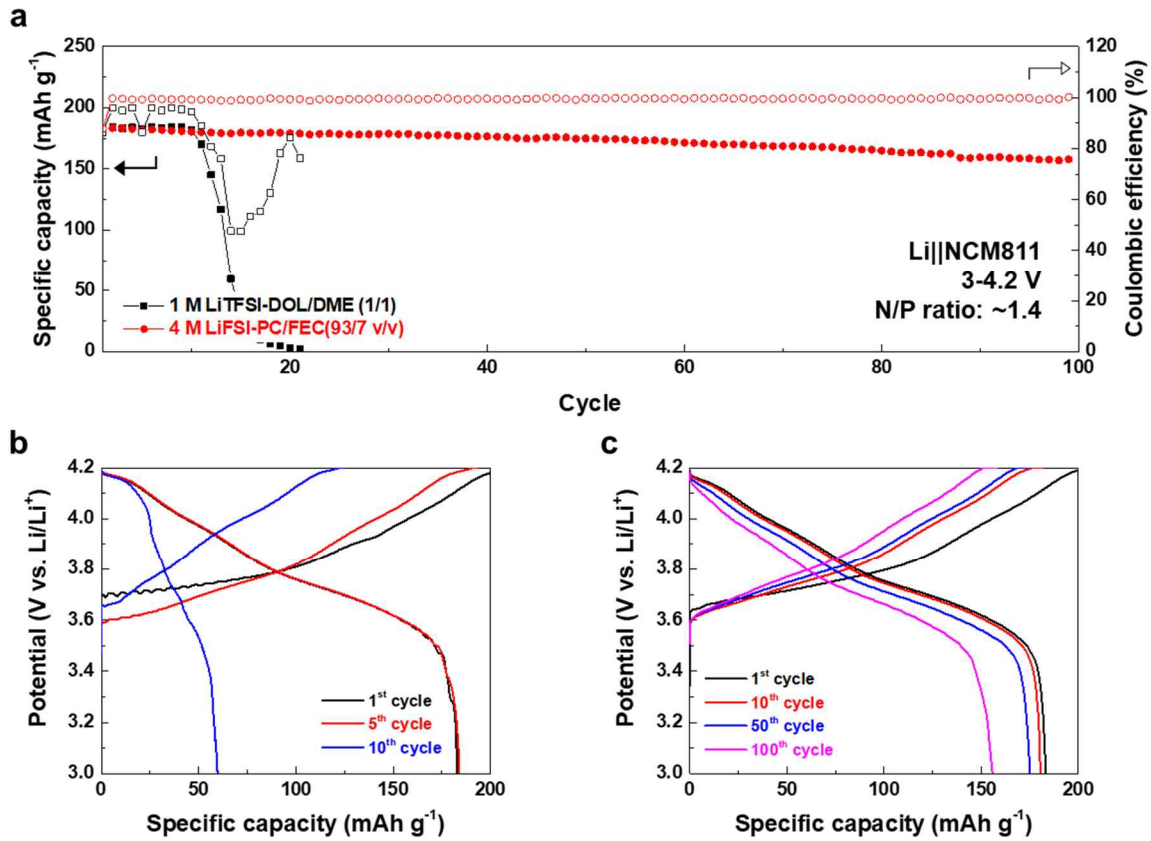

Figure 2.7. Electrochemical behavior of Li||NCM811 full cells with different electrolytes. a. Cycling performance of Li||NCM811 full cells using different electrolytes between 3.0 and 4.2 V. b-c. Voltage profiles of Li||NCM811 full cells at selected cycling during cycling in different electrolytes: 1 M LiTFSI-DOL/DME (b) and 4 M LiFSI-PC/FEC (c).

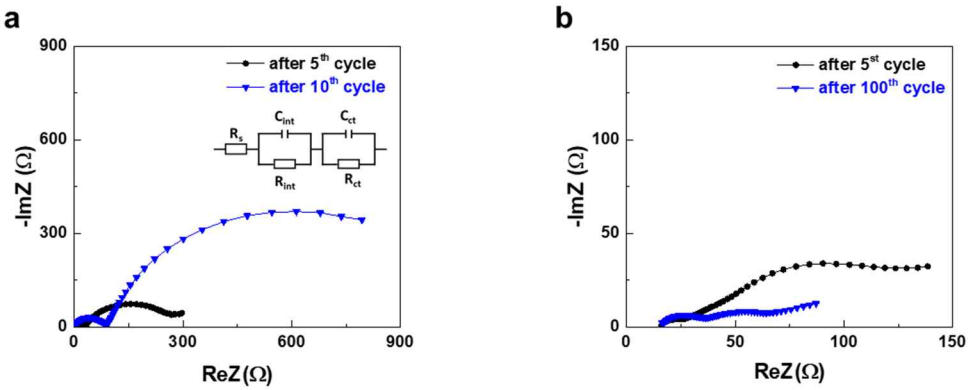

Figure 2.8. Nyquist plots of Li||NCM811 full cells. a-b. Nyquist plots of Li||NCM811 full cells in different electrolytes: 1 M LiTFSI-DOL/DME (a) and 4 M LiFSI-PC/FEC (b) at different stages of cycling. The inset is the equivalent circuit.

To further investigate the effect of 4 M LiFSI-PC/FEC on the NCM811, transmission electron microscope (TEM) characterization was conducted before and after the cycling test. Compared to pristine NCM811, the CEI layers with different thicknesses can be clearly observed on the surface of cycled NCM811 in different electrolytes (Figure 2.9). Thick CEI layer of 20 nm was formed in 1 M LiTFSI-DOL/DME, derived from the severe oxidative decomposition of electrolytes. In contrast, the thickness of the CEI layers are about 8.9 nm for 4 M LiFSI-PC/FEC. This thinner CEI layer would decrease the internal resistance of the cell and resulted in improving the performance of Li||NCM811 cell as observed in Figure 2.7.

The beneficial contribution of the CEI layer formed by 4 M LiFSI-PC/FEC was quantitatively elucidated by examining XPS F 1s spectra. In the case of NCM811 cycled in 1 M LiTFSI-DOL/DME, an evident peak (684.6 eV) assigned to LiF/MnF_2 was observed (Figure 2.10a). The LiF and MnF_2 byproducts are known to be formed *via* undesired side reactions between acidic species, derived from electrolyte decomposition, and dissolved Mn^{2+} ions.[23, 47-48] On the other hand, the NCM811 surface for the 4 M LiFSI-PC/FEC presents unremarked LiF/MnF_2 peak (Figure 2.10b). Such a dramatic difference in the NCM811 surface was further confirmed by analyzing time-of-flight secondary ion mass spectrometry (TOF-SIMS) analysis of $^7LiF_2^-$ (Figure 2.10c). Consistent with the XPS results, the absolute amount of that ions was lower, and they were thinly populated over a wide area at the 4 M LiFSI-PC/FEC, as compared to the 1 M LiTFSI-DOL/DME.

The effect of CEI layer on the interfacial exothermic reaction between the NCM811 and electrolytes was also evaluated by differential scanning calorimetry (DSC) (Figure 2.11a). The NCM811 with 1 M LiTFSI-DOL/DME shows low major exothermic peak temperatures (T_{peak}=220.2 ºC) and a large exothermic heat (ΔH=786.6 J g^{-1}), indicating that intense interfacial exothermic reaction occurred. In contrast, the 4 M LiFSI-PC/FEC considerably improvs the thermal stability. The major exothermic peak temperature shifted to higher temperatures (T_{peak}= 250.9 ºC) and the exothermic heat was also reduced by more than half (ΔH=326.7 J g^{-1}) compared to ether-based electrolyte. These DSC results indicate that the CEI layer formed by 4 M LiFSI-PC/FEC effectively prevents the direct contact of NCM811 surface with electrolyte, thereby alleviating the interfacial exothermic reaction.

In conclusion, XPS, TOF-SIMS and DSC results emphasize the advantageous effect of CEI layer formed by 4 M LiFSI-PC/FEC on suppressing interfacial side reaction between NCM811 and electrolytes.

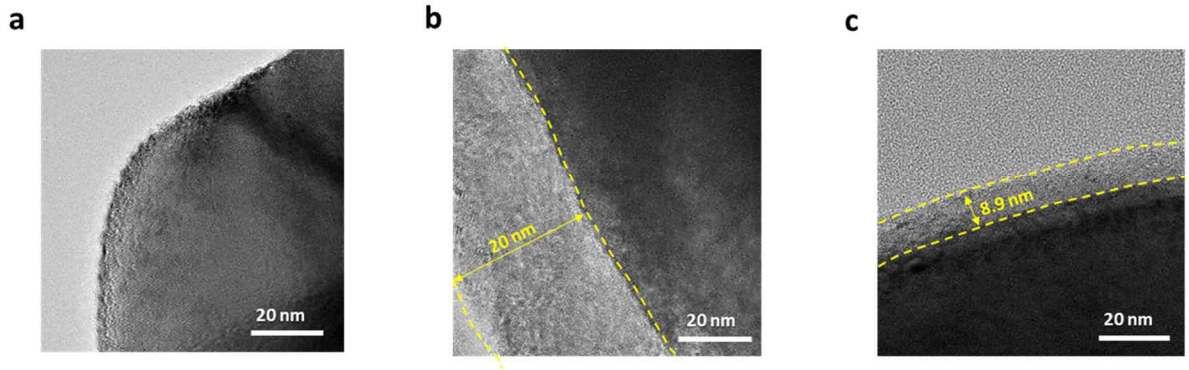

Figure 2.9. HR-TEM images of the NCM811. a. Pristine NCM811. b-c. the cycled NCM811 (after 100th cycle) in different electrolytes: 1 M LiTFSI-DOL/DME (b) and 4 M LiFSI-PC/FEC (c).

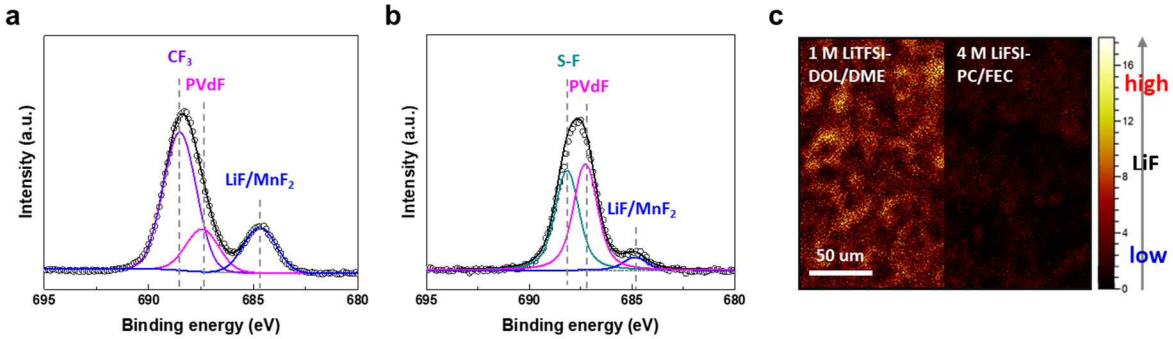

Figure 2.10. Surface analysis performed on cycled NCM811. a-b. XPS spectra of F 1s for CEI layer formed on cycled NCM811 cathodes in 1 M LiTFSI-DOL/DME (a) and 4 M LiFSI-PC/FEC (b). c. TOF-SIMS images of $^{7}LiF_2^-$ on cycled NCM811 cathodes in different electrolytes.

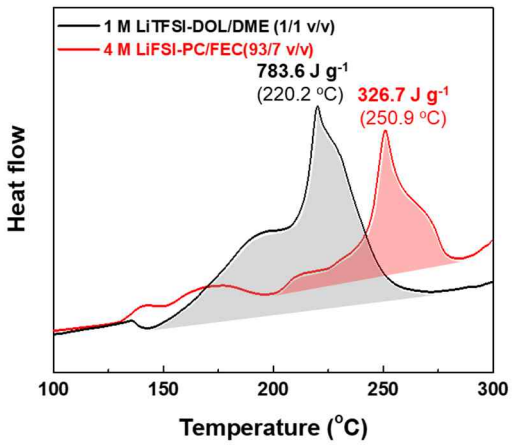

Figure 2.11. DSC curves of interfacial exothermic reactions between electrolytes and delithiated NCM811.

2.3.3. Nonflammable electrolytes for high-safe lithium metal batteries

In addition to the electrochemical benefits contributed by 4 M LiFSI-PC/FEC, another advantage is nonflammability, which is greatly valuable for Li metal batteries but unsatisfied with commercial organic electrolytes. To elucidate thermal stability of the 4 M LiFSI-PC/FEC, isothermal TGA was conducted at 80 ºC (Figure 2.12a). For comparison, ether-based electrolytes (specifically, 1 M LiTFSI-DOL/DME and 4 M LiFSI-DME), which are representative electrolytes for Li metal,[49] were chosen as control samples. 4 M LiFSI-PC/FEC showed negligible weight loss (~ 6 wt%) over elapsed time of 100 min, whereas severe weight loss (~ 65 wt% and ~ 32 wt%) was observed at 1 M LiTFSI-DOL/DME and 4 M LiFSI-DME, respectively. To visualize the volatility of the electrolytes, Al pouch-type cells containing the different electrolytes were fabricated. The cells were subjected to the thermal shock condition (200 ºC/60 min). The top photographs in Figure. 2.12b-d show that the cell incorporating the 4 M LiFSI-PC/FEC remains intact without expansion, in comparison to the control cells that were greatly swollen up due to their high volatile property. Accordingly, the ether-based electrolytes were ignited by the flame, but the 4 M LiFSI-PC/FEC showed nonflammable nature (bottom photographs in Figure 2.12b-d). Concentrated electrolytes are known to show the improvement in thermal stability,[21] however, 4 M LiFSI-DME does not yet reach satisfactory level of thermal stability. From the abovementioned results, it should be noted that the 4 M LiFSI-PC/FEC can be suggested as a nonflammable one to effectively address the safety issue of Li metal batteries.

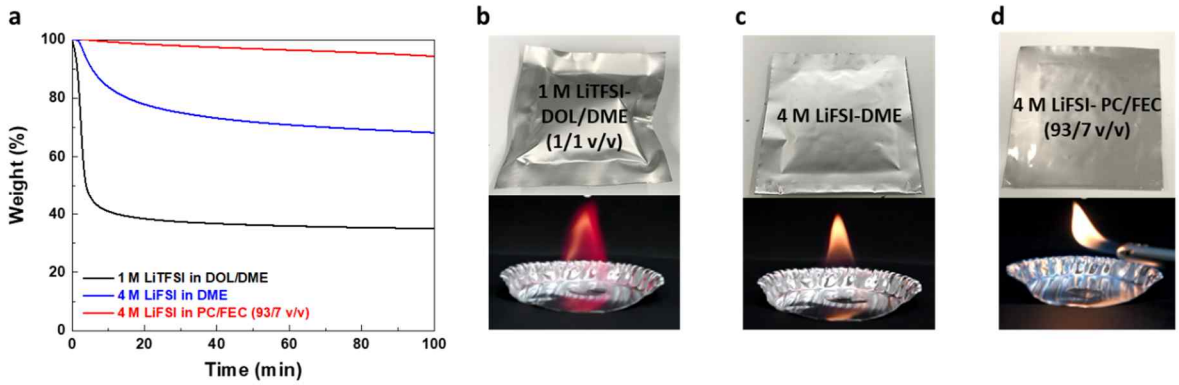

Figure 2.12. Comparison of thermal stability of different electrolytes. a. Weight loss of ether-based electrolytes (1 M LiTFSI-DOL/DME and 4 M LiFSI-DME) and 4 M LiFSI-PC/FEC measured by the isothermal TGA at 80 °C for 100 min. b-d. Photographs showing the volatility (top photographs) and inflammability (bottom photographs) of 1 M LiTFSI-DOL/DME (b), 4 M LiFSI-DME (c) and 4 M LiFSI-PC/FEC (d). The thermal shock test conducted at 200 °C for 60 min.

2.4. Conclusion

In summary, we have designed nonflammable PC-based electrolytes for high-energy density and high-safe Li metal batteries. This electrolyte consists of PC solvents which have excellent thermal and oxidative stability and LiFSI salts which can form a stable SEI layer on the Li-metal. And we also added FEC to further improving the stability of the SEI layer. When the concentration of LiFSI is 4 M, a stable C-N/C-F-rich SEI layer and a thin and stable CEI layer was concurrently formed on both Li-metal and NCM811, effectively inhibiting the interfacial side reactions.

Accordingly, 4 M LiFSI-PC/FEC simultaneously resolved the four most urgent issues faced by such high-energy density Li-metal batteries *via* forming stable passivation layers on the electrodes: (1) reductive side reaction between Li-metal and electrolytes; (2) Li-dendrite formation; (3); oxidative decomposition of electrolytes; (4) transition metal ion dissolutions from NCM811. Benefiting from the combined effects, the Li||NCM811 full cells provide exceptional improvements in electrochemical performance under 3.0 mAh cm^{-2} of high loading cathodes with limited amounts of Li-metal over 100 cycles. In addition, since this electrolyte is nonflammable, we anticipate that it can effectively address the safety issue of Li metal batteries. Accordingly, we envision that this electrolyte will lead us a step closer to the future electric vehicle era.

III. References

1. R. Hausbrand, G. Cherkashinin, H. Ehrenberg, M. Groting and K. Albe, *Materials Science and Engineering: B,* **2015,** *192*, 3-25
2. K. Xu, *Chem. Rev*., **2014**, *114* (23), 11503-11618
3. K. Xu, *Chem. Rev*., **2004**, *104*, 4303-4417
4. M. Ue and S. Mori, *J. Electrochem. Soc*., **1995**, *142* (8), 2577-2581
5. W. Xu and A. Angell, *Electrochem. Solid-State Lett*., **2001**, *4* (1), E1-E4
6. D. Lin, Y. Liu and Y. Cui, *Nat. Nanotechnol.*, **2017**, *12*, 194-206
7. Y. Lu, Z. Tu and L. A. Archer *et al*., *Nat. Mater*., **2014**, *13*, 961-969
8. W. Li, H. Yao, K. Yan, G. Zheng, Z. Liang, Y.-M. Chiang and Y. Cui, *Nat. Commun.*, **2015**, *6*, 7436-7443
9. F. Ding, W. Xu, X. Chen, J. Zhang, M. H. Engelhard, Y. Zhang, B. R. Johnson, J. V. Crum, T. A. Blake, X. Liu and J.-G. Zhang, *J. Electrochem. Soc.*, **2013**, *160* (10), A1894-A1901
10. Y. Li, J. Yang and J. Song *et al*., *Renewable Sustainable Energy Rev.*, **2016**, *54*, 1250-1261
11. Z. Liang, D. Lin, J. Zhao, Z. Lu, Y. Liu, C. Liu, Y. Lu, H. Wang, K. Yan, X. Tao and Y. Cui, *Proc. Natl. Acad. Sci. U.S.A.*, **2016**, *113*, 2862-2867
12. J. Wang, Y. Yamada, K. Sodeyama, E. Watanabe, K. Takada, Y. Tateyama and A. Yamada, *Nat. Energy.*, **2018**, *3*, 22-29
13. G. Zheng, S. W. Lee, Z. Liang, H.-W. Lee, K. Yan, H. Yao, H. Wang, W. Li, S. Chu and Y. Cui, *Nat. Nanotech*., **2014**, *9*, 618-623
14. A. C. Kozen, C.-F. Lin, A. J. Pearse, M. A. Schroeder, X. Han, L. Hu, S.-B. Lee, G. W. Rubloff and M. Noked, *ACS Nano*, **2015**, *9* (6), 5884-5892
15. H. Ye, S. Xin, Y.-X. Yin, J.-Y. Li, Y.-G. Guo and L.-J. Wan, *J. Am. Chem. Soc.*, **2017**, 139 (16), 5916-5922
16. H. Wu, Y. Cao, L. Geng and C. Wang, *Chem. Mater*., **2017**, *29* (8), 3572-3579
17. T.-T. Zuo, X.-W. Wu, C.-P. Yang, Y.-X. Yin, H. Ye, N.-X. Li and Y.-G. Guo, *Adv. Mater.*, **2017**, *29*, 1700389-1700394
18. R. Miao, J. Yang, Z. Xu, J. Wang, Y. Nuli and L. Sun, *Sci. Rep*., **2016**, *6*, 21771-21779

19. E. M. Erickson, E. Markevich, G. Salitra, D. Sharon, D. Hirshberg, I. Shterenberg, A. Rosenman, A. Frimer and D. Aurbach *et al*., *J. Electrochem. Soc.*, **2015**, *162* (14), A2424-A2438

20. S. Hess, M. Wohlfahrt-Mehrens and M. Wachtler, *J. Electrochem. Soc*., **2015**, *162* (2), A3084-A3097

21. Y. Yamada and A. Yamada *et al*., *J. Electrochem. Soc*., **2015**, *162* (14) A2406-A2423

22. X. Fan, L. Chen, X. Ji, T. Deng, S. Hou, J. Chen, J. Zheng, F. Wang, J. Jiang, K. Xu and C. Wang, *Chem*, **2018**, *4*, 174-186

23. S. Jiao, X. Ren, R. Cao, M. H. Engelhard, Y. Liu, D. Hu, D. Mei, J. Zheng, W. Zhao, Q. Li, N. Liu, B. D. Adams, C. Ma, J. Liu, J.-G. Zhang, and W. Xu, *Nat. Energy*., **2018**, *3*, 739-746

24. E. Markevich, G. Saltira, F. Chesneau, M. Schmidt, and D. Aurbach, *ACS Energy Lett*., **2017**, *2* (6), 1321-1326

25. J. Zheng, M. H. Engelhard, D. Mei, S. Jiao, B. J. Polzin, J.-G. Zhang, and W. Xu, *Nat. Energy*., **2017**, *2*, 17012-17019

26. W. Zhao, J. Zheng, L. Zou, H. Jia, B. Liu, H. Wang, M. h. Engelhard, C. Wang, W. Xu, Y. Yang, and J.-G. Zhang, *Adv. Energy Mater*., **2018**, *8*, 1800297-1800305

27. S. Chen, J. Zheng, L. Yu, X. Ren, M. H. Engelhard, C. Niu, H. Lee, W. Xu, J. Xiao, J. Liu, and J.-G. Zhang, *Joule*, **2018**, *2*, 1-11

28. S. Jiao, J. Zheng, Q. Li, X. Li, M. H. Engelhard, R. Cao, J.-G. Zhang and W. Xu., *Joule*, **2018**, *2*, 110-125

29. X. Fan, L. Chen, O. Borodin, X. Ji, J. Chen, S. Hou, T. Deng, J. Zheng, C. Yang, S.-C. Liou, K. Amine, K. Xu and C. Wang, *Nat. Nanotech*., **2018**, *13*, 715-722

30. B. Liu, J.-G. Zhang, and W. Xu, *Joule*, **2018**, *2*, 833-845

31. S.-K. Jeong, H.-Y. Seo, D.-H. Kim, H.-K. Han, J.-G. Kim, Y. B. Lee, Y. Iriyama, T. Abe, and Z. Ogumi, *Electrochem. Commun*., **2008**, *10* (4), 635-638

32. D. M. Seo, O. Borodin, S.-D. Han, P. D. Boyle, and W. A. Henderson, *J. Electrochem. Soc.*, **2012**, *159* (9), A1489-A1500

33. Y. Yamada, C. H. Chiang, K. Sodeyama, J. Wang, Y. Tateyama and A. Yamada, *ChemElectroChem*, **2015**, *2*, 1687-1694

34. J. Wang, Y. Yamada, K. Sodeyama, C. H. Chiang, Y. Tateyama and A. Yamada, *Nat. Commun*., **2016**, *7*, 12032-12040

35. S.-D. Han, O. Borodin, D. M. Seo, Z.-B. Zhou and W. A. Henderson, *J. Electrochem. Soc.*, **2014**, *161* (14), A2042-A2053

36. Y. Yamada, K. Furukawa, K. Sodeyama, K. Kikuchi, M. Yaegashi, Y. Tateyama and A. Yamada, *J. Am. Chem. Soc.*, **2014**, *136*, 5039-5046

37. N. Takenaka, T. Fujie, A. Bouides, Y. Yamada, A. Yamada and M. Nagaoka, *J. Phys. Chem. C*, **2018**, *122*, 2564-2571

38. A. Heckmann, J. Thienenkamp, K. Beltrop, M. Winter, G. Brunklaus and T. Placke, *Electrochim. Acta*, **2018**, *260*, 514-525

39. T. Husch and M. Korth, *Phys. Chem. Chem. Phys.*, *2015*, **17**, 22799-22808

40. Y. Li, K. Leung and Y. Qi, *Acc. Chem. Res.*, **2016**, *49* (10), 2363-2370

41. C. Yang, Y. Yao, S. He, H. Xie, E. Hitz and L. Hu, *Adv. Mater*., **2017**, *29*, 1702714-1702721

42. Q. Pang, X. Liang, A. Shyamsunder and L. F. Nazar, Joule, 2017, 1, 871-886

43. C. Wang, Y. Yang, X. Liu, H. Zhong, H. Xu, Z. Xu, H. Shao and F. Ding, *ACS Appl. Mater. Interfaces*, **2017**, *9* (15), 13694-13702

44. K. N. Wood, M. Noked and N. P. Dasgupta, *ACS Energy Lett*., **2017**, *2* (3), 664-672

45. E. Markevich, G. Salitra, F. Chesneau, M. Schmidt and D. Aurbach, *ACS Energy Lett*., **2017**, *2* (6), 1321-1326

46. L. Suo, W. Xue, M. Gobet, S. G. Greenbaum, C. Wang, Y. Chen, W. Yang, Y. Li and J. Li, *Proc. Natl. Acad. Sci. U.S.A.*, **2018**, *115* (6), 1156-1161

47. D. H. Jang and S. M. Oh, *J. Electrochem. Soc.*, **1997**, *144* (10), 3342-3348

48. J.-M. Kim, J.-H. Park, C. K. Lee and S.-Y. Lee, *Sci. Rep.*, **2014**, *4*, 4602-4608

49. J. Qian, W. A. Henderson, W. Xu, P. Bhattacharya, M. Engelhard, O. Borodin and J.-G. Zhang, *Nat. Commun.*, **2015**, *6*, 6362